Balloon-based measurements of the profile of downwelling shortwave irradiance in the troposphere

D. Hagan,[1] D. Crisp,[1] J.-F. Blavier,[1] L. Di Girolamo,[2] and T. Ackerman[3]

[1]Earth and Space Sciences
Jet Propulsion Laboratory
California Institute of Technology

[2]Institute of Atmospheric Physics
University of Arizona

[3]Department of Atmospheric Science
Pennsylvania State University

Abstract. Using a helium plus reversible fluid balloon system as the observing platform, multiple profiles of shortwave irradiance between 4 and 10 km were recently obtained over the Los Angeles basin. This novel dual balloon system can make repeated excursions through an atmospheric layer as deep as a scale height. In this case, four profiles of downwelling hemispheric broadband irradiance were obtained over a period of six hours in conditions that could be characterized by a mid-latitude, summer model atmosphere. These data are described and compared to model computations using a spectrum-resolving, plane parallel, multiple scattering model. The large systematic difference between model and observations (10%) at the high altitudes is discussed in terms of possible factors that affect the instrument measurement response under cold temperature conditions. However, the results show that downwelling shortwave irradiance in cloud free conditions can be calculated to an accuracy of about 5% in the lower region of the troposphere.

Introduction

The accurate measurement and modeling of processes affecting the transfer of solar radiation through the Earth's atmosphere remains a formidable problem in present climate studies [*Wielicki et al.*, 1995]. This is an especially relevant problem in light of many recent papers which provide evidence for anomalies in the absorption of cloudy and clear sky shortwave radiation [*Ramanathan et al.*, 1995; *Cess et al., 1995*; *Wild et al.*, 1995; *Li et al.*, 1995; *Pilewskie and Valero*, 1995 *Charlock and Alberta*, 1996]. The discrepancy between models and observations, which varies from 5 to 30%, is often attributed to errors in measuring and modeling the diffuse component of the incoming shortwave radiation.

Recently, intensive experiments have been undertaken to measure the variables needed to compute the vertical profile of shortwave fluxes [*Charlock and Alberta*, 1996]. One remaining challenge is to obtain high quality *in situ* measurements of the vertical fluxes to validate the radiative transfer models. Here, we describe a new approach for measuring the vertical profile of solar radiation in the troposphere that employs robotic balloons or aerobots as the observing platform. Aerobots are able to make repeated excursions over an

atmospheric scale height using helium plus reversible fluid balloon technology [*Jones*, 1996].

In this study, aerobot-based observations of broadband solar irradiance are interpreted using a spectrum-resolving plane parallel multiple scattering model [*Crisp*, 1997]. The measurements and model relationships are explored and interpreted in this Lagrangian observing system, and found to be well understood in clear sky conditions.

Measurement Technique

Robotic aerovehicles, or "aerobots", employ new advanced altitude control capabilities, which differ significantly from the ballast and valve techniques used by conventional balloons. Several types of aerobots have been designed for *in situ* measurements in planetary atmospheres [*Nock et al., 1996*]. One type is based on the use of reversible fluid buoyancy control to achieve predetermined cyclical altitude variations [*Jones*, 1996]. A closed-system reversible fluid balloon uses the naturally occurring atmospheric temperature variation with altitude to provide the mechanical energy needed for altitude change (Figure 1). The reversible fluid used is selected such that the transition point of the phase change, which depends on the ambient pressure and temperature, will occur within the altitude range of interest. For conditions in which the temperature decreases with increasing altitude, the phase change of the fluid is used to control the buoyancy of a balloon system. When the reversible fluid is in the gas phase, the balloon has a lower average density than the surrounding atmosphere, thus providing a net increase in lift (Figure 1a). Conversely, when the fluid is in the liquid phase, the balloon has a higher average density than the surrounding atmosphere thus providing negative lift. Hence, the aerobot cycles about the equilibrium altitude of the phase change, and is capable of making multiple excursions over an atmospheric scale height.

Over the past several years, these balloons have been tested successfully during a series of flights called the Altitude Control Experiment (ALICE). The balloon systems have a small total payload mass (<3 kg) and use a buoyancy control bag containing commercial

refrigerant fluid mixtures tethered to a helium balloon. Fluid boiling at low altitudes is facilitated by an integrated heat exchanger in the condenser bag. An example of the aerobot configuration and dimensions is shown in Figure 1b. A radiosonde package is located between the reversible fluid bag and the helium balloon. Figure 1c shows the predicted versus actual aerobot trajectory for the first tropospheric radiation science flight, the results of which are reported here.

Description of Aerobot Data

On September 29, 1996, an aerobot carrying an up-looking Eppley pyranometer and radiometer orientation sensors was released at the Jet Propulsion Laboratory (JPL) in Pasadena, California. The objective of the flight was to obtain multiple profiles of shortwave irradiance over the course of the day to test the capability of this new type of platform for observations of the atmospheric radiation field. The Eppley instrument was mounted on a styrofoam plate, attached to the top of the helium balloon. The pyranometer measures global solar radiation, which includes the direct beam of incoming sunlight and the diffuse component due to scattering. Attitude sensors which included a flux gate compass and dual-axis clinometer were placed near the pyranometer. The pyranometer measurements and attitude information were transmitted by radio frequency to ground-based receivers, using a commercial radiosonde as the data link. The radiosonde also made measurements of atmospheric pressure, temperature and relative humidity.

The aerobot was launched from JPL around 9:30 a.m. local time, and performed three full cycles between 4 and 10 km over a horizontal distance of about 200 km (Figure 1c). Two of the cycles were completed during daylight hours. Figure 2 shows the flight altitude and solar zenith angle over the course of the day. The minimum in solar zenith angle was reached when the aerobot had completed the first cycle. The stability of the platform can be characterized by the platform orientation information (Figures 3a-b). The mean tilt of the platform remained near 2^{o} for the duration of the flight. The platform rotated equally in both directions at a typical azimuthal rate of about $5^{o}\ s^{-1}$.

Figure 3c shows the raw Eppley data series, and Figure 3d these data corrected for effects of instrument orientation relative to the direction of the Sun. The geometrical correction accounts primarily for changes in the irradiance with respect to platform tilt [*Banneher and Glover*, 1991]. Strictly speaking, the correction is only valid for measurements of the direct component of the total irradiance. Geometrical corrections for the diffuse component must be treated separately. Although separate measurements of the diffuse irradiance component were not obtained, the results of Figure 3d show the variance of the Eppley data is reduced, without introducing an offset from the mean uncorrected value (Figure 3c).

The Eppley instrument is absolutely calibrated [*Drummond and Greer*, 1966] and traceable to World Standard Instrumentation (WMO IPC VIII Report, 1995). There are several sources of instrument error that combine to result in a nominal accuracy of 5%. These sources of error include: detector linearity (0.5%), electronic component tolerance (1%), temperature compensation of the detector (1-3%), and second-order departures of the detector from cosine (0.5%). As discussed in the modeling section, the first order departure of the detector from a true cosine is directly incorporated into the model. This is a large effect, the relative sensitivity of the detector decreasing from 1 to 5%, for zenith angles between 37 and 60°. For model comparisons, there is another potential source of uncertainty of about 1% in defining the spectral response function of the pyranometer. The temperature compensation of the thermopile was derived for an instrument in thermal equilibrium, and optimized at 263 K. As the instrument moves away from this temperature, the relative sensitivity decreases. The temperature compensation of the detector is a calibrated response, and can be corrected using measurements of the detector substrate temperature. However, the radiosonde used in this experiment did not have enough channels to transmit measurements of the pyranometer temperature.

It is not likely that the instrument ever reached thermal equilibrium, and a separate temperature affect may have been related to a temperature difference between the thermopile

and inner dome. *Albrecht and Cox* [1977] report that during a cold blackbody calibration (near 273 K), the dome temperature of an Eppley pyrgeometer cooled more quickly than the thermopile substrate, and took a few minutes to stabilize at a temperature about 2 K colder than the substrate temperature. We would expect similar behavior from the pyranometer. The temperature difference between the inner dome and thermopile would tend to increase as the instrument moves up and the clear sky becomes darker. This is not a negligible effect, and would be proportional to $\sigma(\varepsilon_d T_d^4 - \varepsilon_t T_t^4)$, where ε_d and ε_t are the emissivities of the inner dome and thermopile, σ the Stefan-Boltzmann constant, and T_d and T_t, the dome and thermopile temperatures. Assuming ε_d and ε_t are near unity in the infrared, and a thermopile temperature of 300 K, this would represent a 6 Wm^{-2} K^{-1} change in the response of the detector.

There are additional concerns in terms of the response of the instrument to the environment. If condensation were to occur on the outer dome, it would diffuse the incoming irradiance and lower the instrument response. Also, as the balloon rose, the instrument was moving further away from the calibration conditions. The energy of the artifical sky source used in the calibration is not the same in spectral distribution as the Sun at the Earth's surface. The calibration of the Eppley pyranometer for outdoor use is accomplished through the adoption of a reference standard that has identical response with respect to wavelength [*Drummond and Greer*, 1966]. While this approach would remove most effects related to wavelength dependence at the surface, there may be a small unknown error due to changes in the spectral distribution of the Sun with height.

Model Description

The radiative transfer model used here incorporates a multi-level, multi-stream, discrete ordinate multiple scattering model, and high resolution spectral mapping methods to provide a description of the radiation field in a plane-parallel, scattering, absorbing, emitting, planetary atmosphere. A brief synopsis of the model is provided here. A more detailed description can be found in *Crisp* [1997] and references therein.

Model calculations were carried out over wavelength regions which matched the spectral response bandwidth of the instrument. Assuming an almost square bandpass, the glass domes on the Eppley define the approximate points of 50% transmission at 4000 and 33000 cm^{-1}. In addition, an adjustment was applied to the model calculations to account for the deviation of the instrument detector response from a true cosine. This response function was derived from a polynomial fit to laboratory measurements obtained from *Michalsky et al.* (1995).

A line-by-line model was used to generate gas absorption coefficients for H_2O, CO_2, N_2O, NO_2, CH_4, O_3, and O_2 at 62 levels between the surface and 80 km (Crisp, 1977), using line parameters from the HITRAN 96 database [*Rothman et al.*, 1992]. H_2O continuum absorption was included using the far-wing line shape function described by *Clough et al.* [1989]. The wavelength-dependent optical properties of aerosols were derived from refractive index data compiled by E. P. Shettle (included on the HITRAN 96 CD ROM). A background aerosol mixture, with a population composed of ammonium sulfates (48%), carbon (2%), water soluble aerosol and dust (each 25%), and in the boundary layer, equal amounts of sea salt and ammonium sulfate, was compiled from various sources [*Crisp*, 1997, and references therein]. The aerosol distribution included a background population with constant number densities between the surface and tropopause. The boundary layer aerosol population had number densities that decreased rapidly with increasing altitude [*Jaenicke*, 1993]. The particle size distributions for the background and boundary layer aerosols were based on the tri-modal, log-normal distributions described by *Jaenicke* [1993].

The model calculations, based on the *McClatchey et al.* [1972] summer mid-latitude atmosphere and gas mixing ratios, include Rayleigh scattering, absorption effects by water vapor and the trace gases, urban mass mixing ratios for NO_2 and O_3 (*Turco*, 1997), and background aerosol with an optical depth of 0.1. The aerobot radiosonde air temperature and relative humidity measurements did not differ significantly from the standard

atmosphere. The calculations were carried out at multiple solar zenith angles ranging between 60 and 37 degrees for direct comparisons with the observations at specific times of day.

Observed Versus Modeled Shortwave Irradiance Profiles

The shortwave irradiance profiles corresponding to two aerobot cycles are shown as a continuous function of time in Figure 4. The fluctuation in the Eppley data is about 1%. Most of the fluctuation can be attributed to platform motion effects that were not compensated by the geometrical correction.

A set of model points derived from the 4-stream multiple scattering calculations are compared to the observations in Figure 4. The model and observed irradiance are within approximately 5% over most of the altitude range, except in the vicinity of points marked by letters g and k, where modeled and observed values differ by almost 10%. The location of this larger discrepancy is more apparent in Figure 5. In this case the solar irradiance is shown as a function of altitude, using the same set of model comparison points. The largest discrepancy between model and observed irradiance occurs at the high altitudes, and is more pronounced during the second excursion of the aerobot (Figure 5b). The associated altitude and zenith angle for each point can be found in Figure 6.

While realistic estimates for the atmospheric gas and aerosol contributions were used in the modeling, the model may be biased higher than the observations because one or more of the model parameters were not correctly estimated or distributed. Moisture condensation on the dome may be another factor in the disagreement between the measured and modeled irradiance profiles. If condensation had occurred, the effects should have been greater during descent, as the instrument moved into warmer air. The larger discrepancies occur during ascent.

Cirrus may have also had an effect on the measurements. At the beginning of the aerobot flight, there were no apparent clouds in the Los Angeles region from satellite or ground views. However, thermal infrared GEOS imagery shows the presence of a high

cirrus cloud moving into the Los Angeles region later in the day. The cloud feature, with an estimated optical depth between 1 and 2, was in closest proximity to the aerobot between 2:00 and 3:00 p.m. local time (Pacific Daylight Time). By this time of day, the aerobot had reached the second altitude peak and was moving back down. Since the discrepancy between model and observations occurs during both aerobot cycles, cirrus could not account for the systematic difference.

We believe the uncertainty in the instrument response due to cooling of the dome, combined with the known instrument errors of 5%, is enough to bridge the observed discrepancy between the observed and calculated shortwave irradiance. For example, a 5% error in the measured shortwave irradiance at 10 km due to a temperature difference between dome and thermopile would only require a ΔT of 7-10 K, for thermopile temperatures ranging between 300 and 250 K. It is not unreasonable to expect temperature gradients of this magnitude to occur, considering that the aluminum housing of the pyranometer was shielded from the Sun, and was insulated from the ambient air by a styrofoam cover. In addition, the air speed of the balloon was slow. The systematic decreases with height in the observed irradiance are consistent with this kind of temperature sensitivity.

Summary

A flight experiment using a new atmospheric profiling method was recently conducted over the Los Angeles basin. The main objective was to test the capability of an aerobot system as a platform for measurements of the tropospheric solar radiation field. An instrument for measuring hemispheric downwelling solar irradiance was placed on top of the upper helium-filled balloon of the dual balloon system. During its transect over the Los Angeles basin, four profiles were made by the aerobot during daylight hours. Over this period, the average change in platform tilt was approximately 2^{o}. The variation in the irradiance due to larger, instantaneous tilt changes could be significantly reduced using platform orientation measurements in a geometrical correction procedure.

The observations have been compared to model calculations using a spectrum-resolving plane parallel multiple scattering model and best guesses for the gas and aerosol contributions, and found to agree to within 5% over much of the lower altitude range. The best agreement occurs where the diffuse component of the total irradiance is the largest. The larger systematic differences at high altitudes could be attributed to known pyranometer measurement errors along with cooling of the instrument dome.

To our knowledge, this is the first time that the same instrument and observing platform have been used to obtain precise, multiple, tropospheric profiles of downwelling solar irradiance by method of continuous vertical profiling. Clearly, the accuracy of the measurements can be improved in future profiling experiments. This can be accomplished with temperature measurements of the instrument housing, detector substrate and dome. The interpretation of the data and comparisons with the model can be improved with measurements of the diffuse component of the irradiance, and some spectral discrimination. The experiment would greatly benefit from ground-based measurements of the vertical profile of cloud and aerosol.

Acknowledgments. The authors would like to acknowledge with thanks the JPL Planetary Aerobot Team for their successful balloon mission design, operation and recovery, and Robert West, Barney Farmer, Mark Foote and Chris Webster for many helpful discussions. This work was supported by the JPL Director's Research and Development Fund.

References

Albrecht, B. and S. K. Cox, Procedures for improving pyrgeometer performance, *J. Appl. Meteor.*, 16, 188-197, 1977.

Bannehr, L. and V. Glover, Preprocessing of airborne pyranometer data, NCAR Technical Note, NCAR/TN-364+STR, 35 pp., 1991.

Cess, R., M. Zhang, P. Minnis, L. Corsetti, E. Dutton, B. Forgan, D. Garber, W. Gates, J. Hack, E. Harrison, X. Jing, J. Kiehl, C. Long, J. Morcrettte, G. Porter, V. Ramanathan, B Subsilar, C. Whitlock, D. Young, Y. Zhou, Absorption of solar radiation by clouds: observations versus models. *Science*, 267, 496-499, 1995.

Charlock, T.P. and T. L. Alberta, The CERES/ARM/GEWEX Experiment (CAGEX) for the retrieval of radiative fluxes with satellite data, *Bull. Amer. Meteor. Soc.*, 7, 2673-2683, 1996.

Clough, S. A., F.X. Kneizys and R.W. Davies, Line shape and the water vapor continuum, *Atmospheric Res.*, 23,229-241, 1989.

Crisp, D., Absorption of sunlight in clear and cloudy atmospheres: a solution to the cloud absorption anomaly? submitted for publication, 1997.

Drummond, A. J. and H. W. Greer, Integrating hemisphere (artificial sky) for the calibration of meteorological pyranometers, *Solar Energy*, 10, 7-11, 1966.

Jaenicke, R., Tropospheric aerosols, *Aerosol-Cloud-Climate Interactions* ed. P. V. Hobbs, (Academic Press, Inc., San Diego), 1-31, 1993.

Jones, J., Reversible fluid balloon altitude control concepts, *Proceedings of the 11th Lighter-Than-Air Systems Tech. Conf, AIAA-95-1621*, Clearwater, Fl, May 1996.

Li, Z., H. Baker, and L. Moreau, The variable effect of clouds on atmospheric absorption of solar radiation. *Nature*, 376, 486-490, 1995.

McClatchey, R., R. Fenn, J. Selby, F. Voltz, and J. Garing, Optical properties of the atmosphere (revised), *Environ. Res.* Paper 354, 110 pp., 1972.

Michalsky, J., L. Harrison and W. Berkheiser, Cosine response characteristics of some radiometric and photometric sensors, *Sol. Energy*, 54, 397-402, 1995.

Nock, K., J. Jones, G. Rodriguez, Planetary aerobots: a program for robotic balloon exploration, *Proceedings of the 11th Lighter-Than-Air Systems Tech. Conf, AIAA-95-1621*, Clearwater, Fl, May 1996.

Pielewskie, P. and F. Valero, Direct observations of excess solar absorption by clouds, *Science*, 267, 1626-1629, 1995.

Ramanathan, V., B. Subasilar, G. Zhang, W. Conant, R. Cess, J. Kiehl, H. Grassl, L., M., A. Shi, Warm pool heat budget and shortwave cloud forcing: a missing physics? *Science*, 267, 499-503, 1995.

Rothman, L. S., R.R. Gamache, R. H. Tipping, C.P. Rinsland, M.A.H. Smith, D. Chris Benner, V. Malathy Devi, J.-M. Flaud, C. Camy-Peyret, A. Perrin, A. Goldman, S.T. Massie, L.R. Brown, and R. A. Toth, The Hitran molecular database: Editions of 1991 and 1992, *J. Quant. Spectrosc. Radiat. Transfer*, 48, 469-507, 1992.

Turco, R., Earth under siege. From air pollution to global change, Oxford University Press, 527 pp., 1997.

Wielicki, B.A., R.D. Cess, M.D. King, D.A. Randall and E.F. Harrison, Mission to Planet Earth: Role of clouds and radiation in climate, *Bull. Amer. Meteor. Soc.*, 76, 2125-2153, 1995.

Wild, M., A. Ohmura and H. Gilgen, Validation of general circulation model radiative fluxes using surface observations, *J. Climate*, 8, 1308-1324, 1995.

World Meteorological Organization International Pyroheliometric Comparison IPC VIII, 25 September - 13 October, 1995, Working Report No. 188, Swiss Meteorological Institute, Davos and Zurich, May 1966.

Figure Captions

Figure 1. Since 1994, repeated excursions of aerobots over an atmospheric scale height have been successfully attained using helium plus reversible fluid balloon technology, during the Altitude Control Experiments (ALICE). The aerobot trajectory shown in the lower panel corresponds to the shortwave irradiance flight on September 29, 1996.

Figure 2. (**a**) aerobot altitude over an 8.5 hour period, (**b**) and solar elevation angle.

Figure 3. (**a**) Aerobot platform tilt, (**b**) azimuthal spin rate of the platform, (**c**) raw Eppley irradiance measurements, (**d**) and same Eppley series with geometrical correction using platform orientation data.

Figure 4. Observed downwelling solar irradiance and model computations (solid dots) versus time of day. Modeled points derived using mid-latitude summer atmosphere temperature and gas mixing ratios, and realistic background aerosol.

Figure 5. Irradiance profiles obtained from measurements compared to modeled values (solid dots) versus height, for the (**a**) morning and (**b**) afternoon ascent-descent cycles of the aerobot. The bars show the percentage of known instrument uncertainty, not including effects of temperature inhomogeneity.

Figure 6. Solar zenith angle versus altitude, showing points at which the model has been evaluated.

a. REVERSIBLE FLUID ALTITUDE CONTROL TECHNIQUE

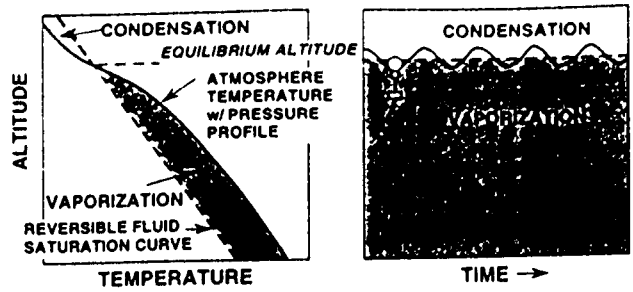

b. ALICE FLIGHT CONFIGURATION

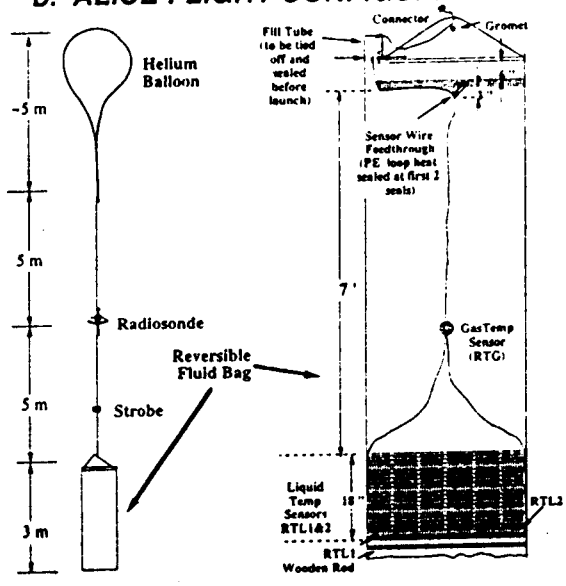

c. ALICE FLIGHT TRAJECTORY (model v. actual)

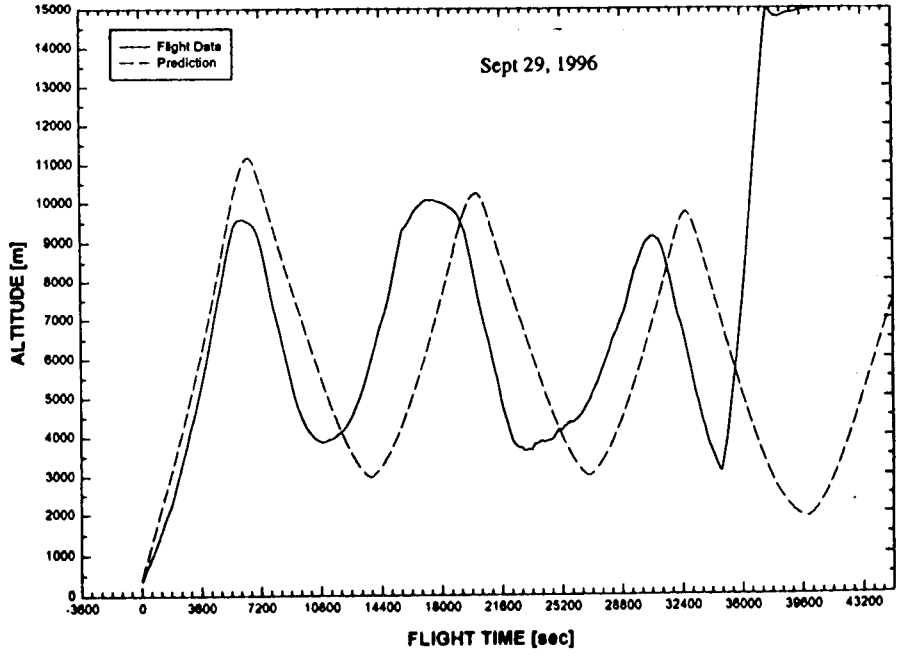

Figure 1

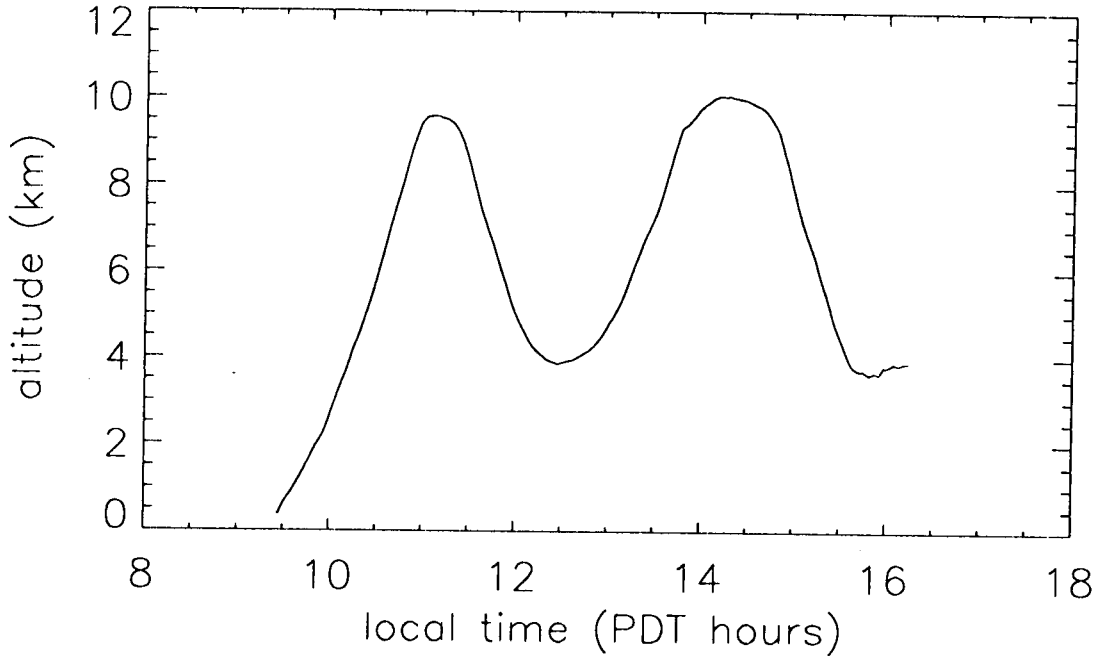
altitude (km)
0
2
4
6
8
10
12
8
10
12
14
16
18
local time (PDT hours)

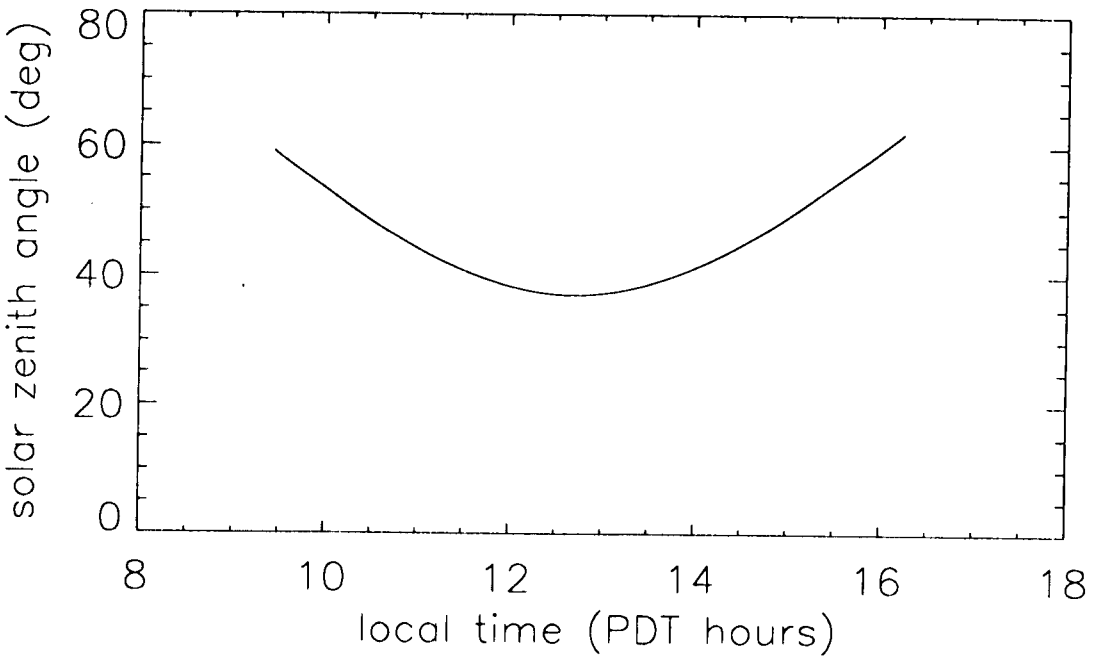
solar zenith angle (deg)
0
20
40
60
80
8
10
12
14
16
18
local time (PDT hours)

Figure 2

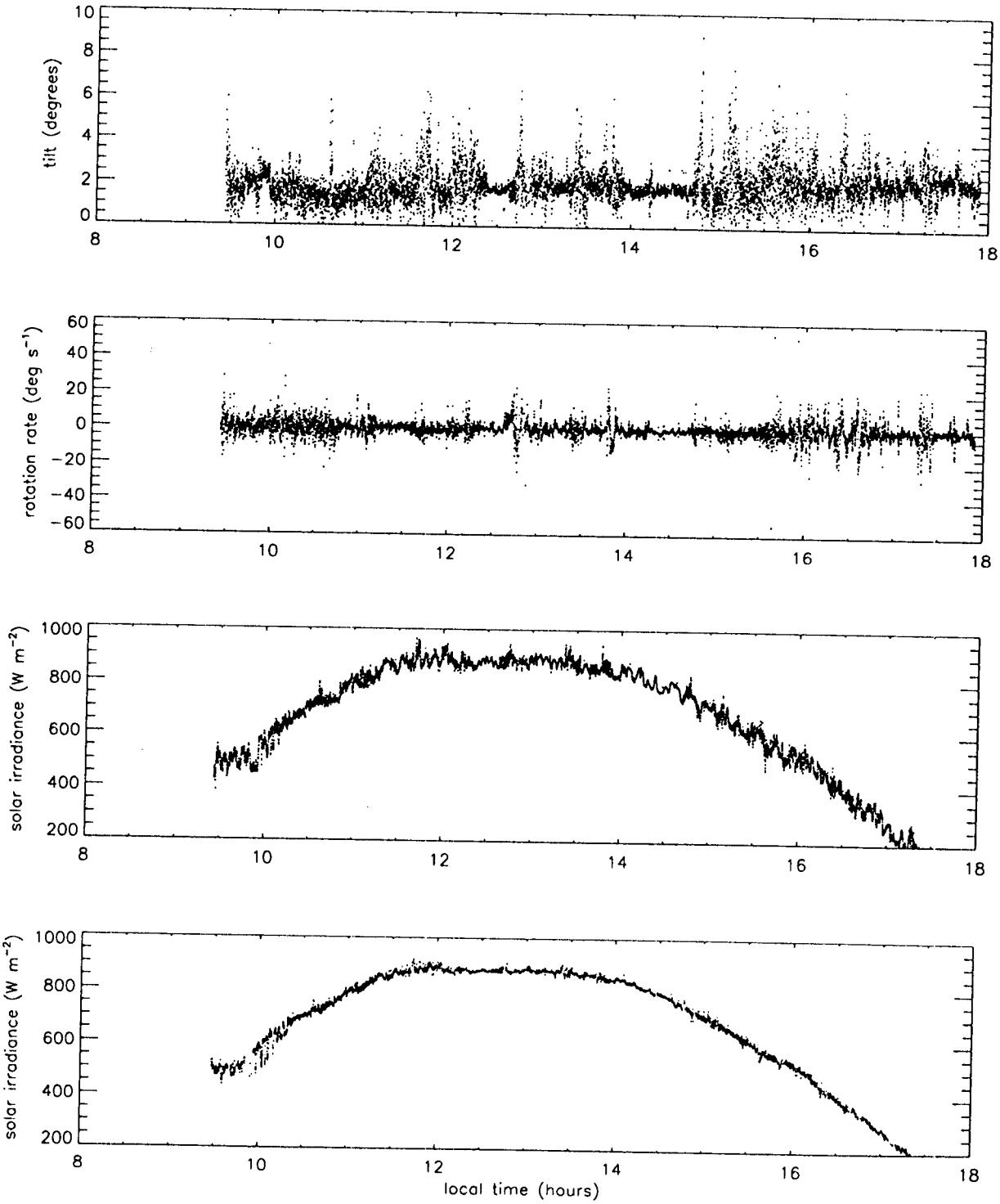
tilt (degrees)
rotation rate (deg s^{-1})
solar irradiance (W m^{-2})
solar irradiance (W m^{-2})
local time (hours)

Figure 3

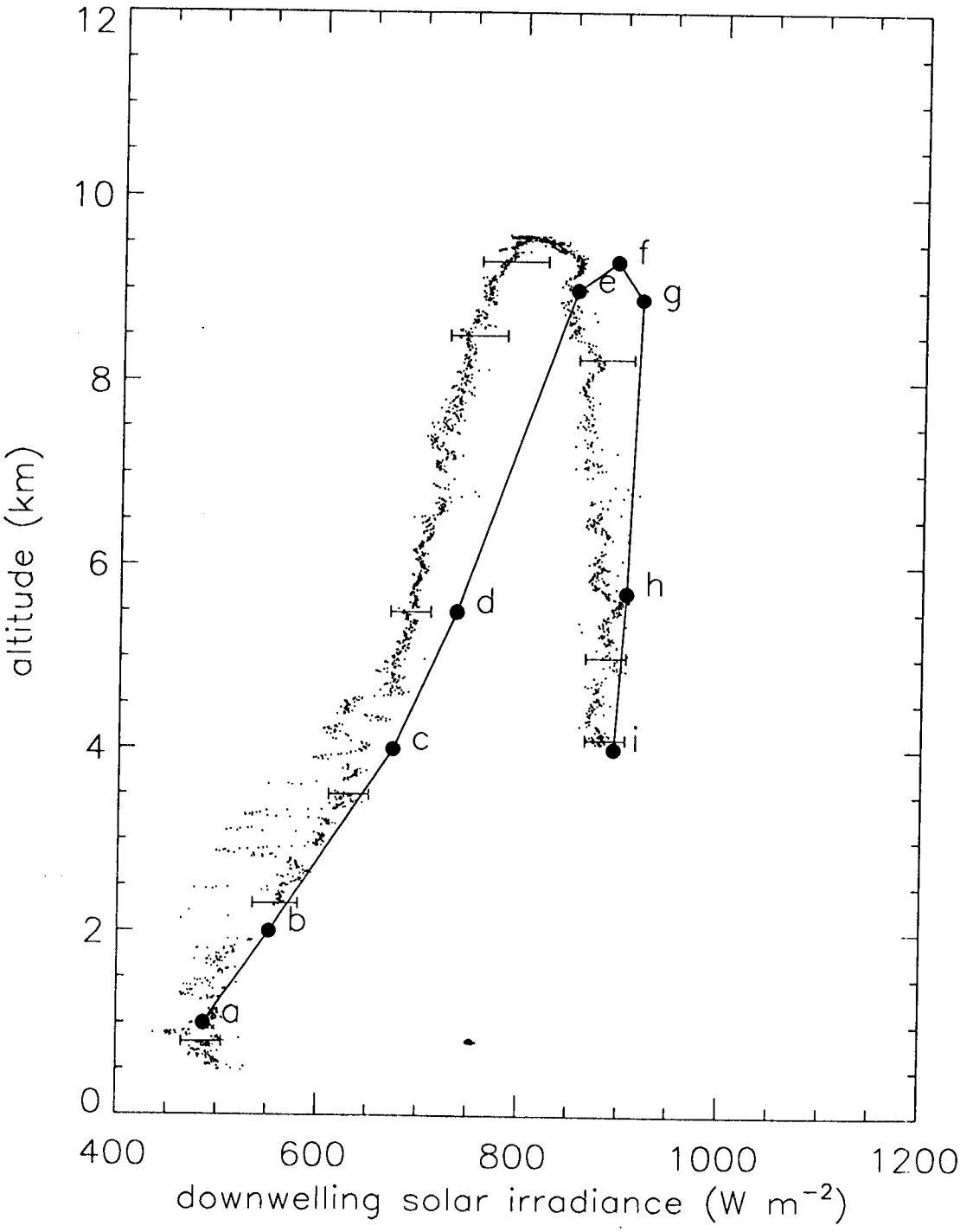
12
10
8
6
4
2
0
altitude (km)
400
600
800
1000
1200
downwelling solar irradiance (W m^{-2})
a
b
c
d
e
f
g
h
i

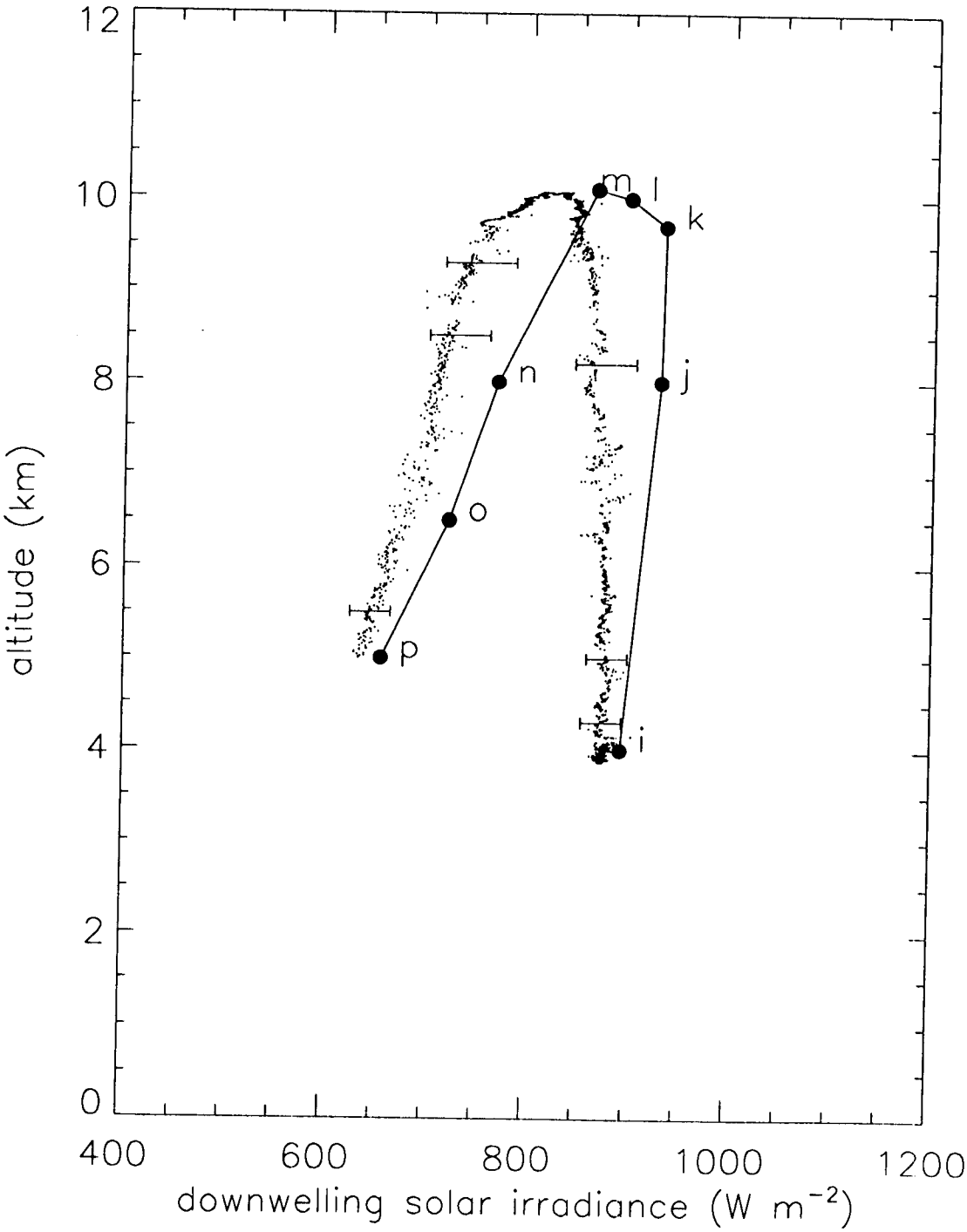
12
10
8
6
4
2
0
altitude (km)
400
600
800
1000
1200
downwelling solar irradiance (W m^{-2})
m
l
k
j
n
o
p
i

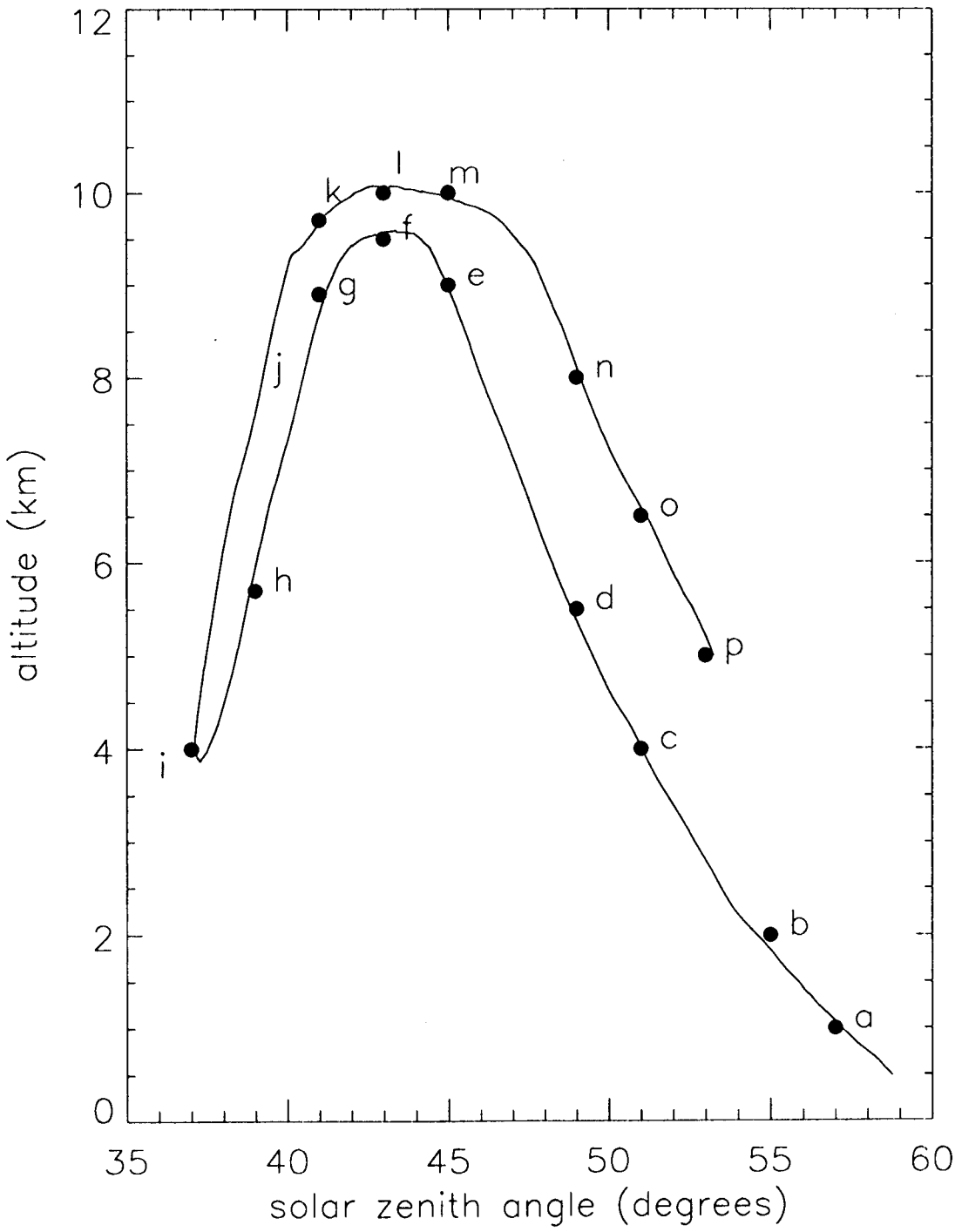
12
10
8
6
4
2
0
altitude (km)
35
40
45
50
55
60
solar zenith angle (degrees)
i
j
k
l
m
n
o
p
h
g
f
e
d
c
b
a